THE JOURNAL OF PHYSICAL CHEMISTRY A
A JOURNAL OF THE AMERICAN CHEMICAL SOCIETY

pubs.acs.org/JPCA Article

Experimental and Theoretical Studies of Dimers Stabilized by Two Chalcogen Bonds in the Presence of a N···N Pnicogen Bond

Mariusz Michalczyk,* Magdalena Malik,* Wiktor Zierkiewicz, and Steve Scheiner

Cite This: J. Phys. Chem. A 2021, 125, 657−668 Read Online

ACCESS | Metrics & More | Article Recommendations | Supporting Information

ABSTRACT: The structure of the 5,6-dichloro-2,1,3-benzoselenadiazole homodimer, obtained by adding the ligand, 4,5-dichloro-*o*-phenylenediamine, to the methanolic solution of $SeCl_4$, was determined by X-ray crystallography, augmented by Fourier transform infrared, Raman, and NMR spectroscopy. The binding motif involves a pair of Se···N chalcogen bonds, with a supplementary N···N pnicogen bond. Quantum calculations provide assessments of the strengths of the individual interactions as well as their contributing factors. All together, these three bonds compose a total interaction energy between 5.4 and 16.8 kcal/mol, with the larger chalcogen atom associated with the strongest interactions. Replacement of the Se atoms by S and Te analogues allows analysis of the dependence of these forces on the nature of the chalcogen atom. Calculations also measure the importance to the binding of the presence of a second N atom on each diazole unit as well as the substituted phenyl ring to which it is fused.

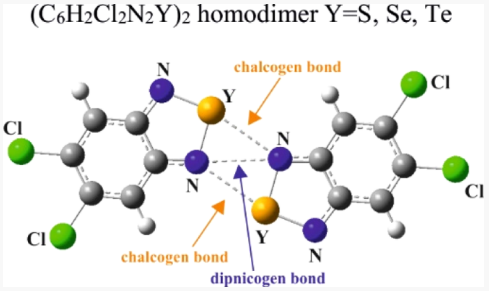

1. INTRODUCTION

Noncovalent interactions represent one of the most intensely studied areas of modern chemistry. Their ubiquitous importance has been documented in a widely diverse set of studies broadly covering biochemistry, catalysis, materials chemistry, and crystal engineering.[1−13] In the latter context, noncovalent interactions are crucial to the stabilization of the crystal subunits and aid formation of the supramolecular synthons. The structural patterns steered by noncovalent interactions which help to organize the higher architectures of complex compounds have been reported in numerous works that continue up to the present.[11,14−20] The hydrogen bond is inarguably the most extensively studied of these noncovalent interactions. H-bonding occupies a special place because of its important role in basic processes responsible for upholding life on earth. The various characteristics of this important interaction have been thoroughly examined in countless publications.[10,21−26]

On the other hand, other closely related noncovalent bonds, such as the halogen bond (XB), have undergone relatively less scrutiny, although this problem is currently being remedied.[27] The halogen bond, like many of its cousins, is characterized first by a small positive region on the outer surface of an electronegative atom bearing a total partial negative charge.[28,29] This region of positive electrostatic potential, commonly labeled as a σ-hole, acts as a binding zone for an approaching Lewis base.[30−32] This idea is not limited to XBs but is common to a number of similar sorts of interactions,[33] baptized according to the name of the element group in the periodic table, such as chalcogen, pnicogen, tetrel, triel, or aerogen bonds.[34−38]

In particular, the chalcogen bond (YB) refers to the Lewis acid−Lewis base noncovalent interaction involving elements of group 16 of the periodic table (mainly the S, Se, and Te atoms and, less frequently, O and Po). The term "chalcogen bond" was introduced by Wang, Ji, and Zhang in 2009[39] and quickly spread to the point where it has been recently and precisely defined by an IUPAC commission.[40] As with its related sister noncovalent bonds, the σ-hole appears along the extension of the R−Y covalent bond axis[34] (where R refers to a generic substituent) and helps to yield the high directionality of chalcogen bonded complexes. The YB strength is determined by a number of factors, including the nature of the substituents, the polarizability, and electronegativity of Y, as well as the basicity of the attacking nucleophile.[34] Generally, YB complex stability increases with the larger Y size: O < S < Se < Te.[1,34] Unlike the XB, where a single σ-hole appears opposite the single R−X bond, the divalent and higher bonding around a Y atom leads to more than one such σ-hole and can likewise lead to a certain degree of steric crowding[1,34] that opposes the nucleophile approach.

A proper understanding of chalcogen bonding has been found to be essential to clarification of a variety of fields such as catalysis,[9,12,41] design of new materials,[42,43] protein folding,[7,44] and anion recognition.[45] Due to its high

Received: December 3, 2020
Revised: December 23, 2020
Published: January 11, 2021

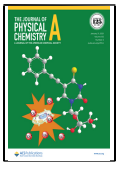

https://dx.doi.org/10.1021/acs.jpca.0c10814
J. Phys. Chem. A 2021, 125, 657−668

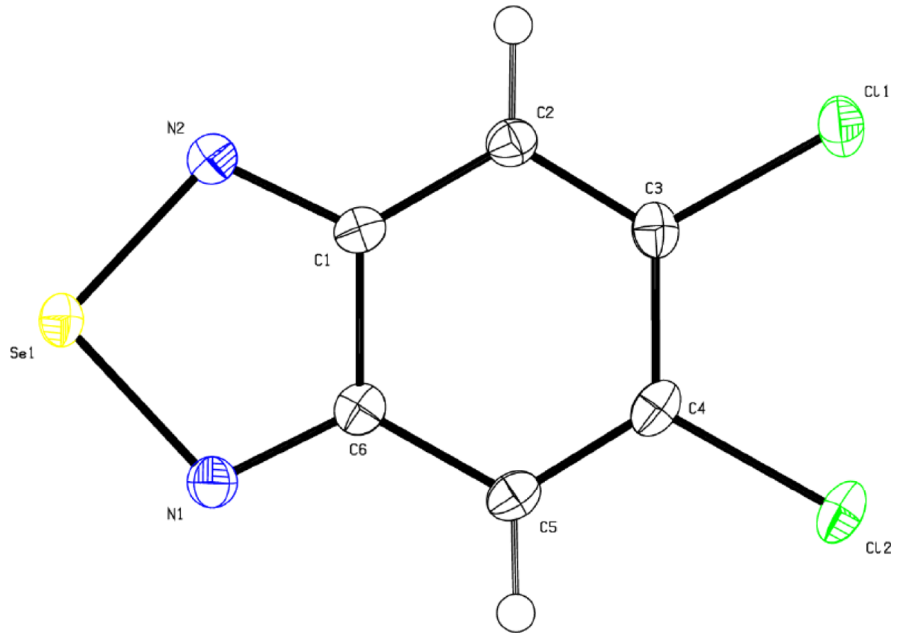

Figure 1. Molecular structures of 5,6-dichloro-2,1,3-benzoselenadiazole together with the atom numbering.

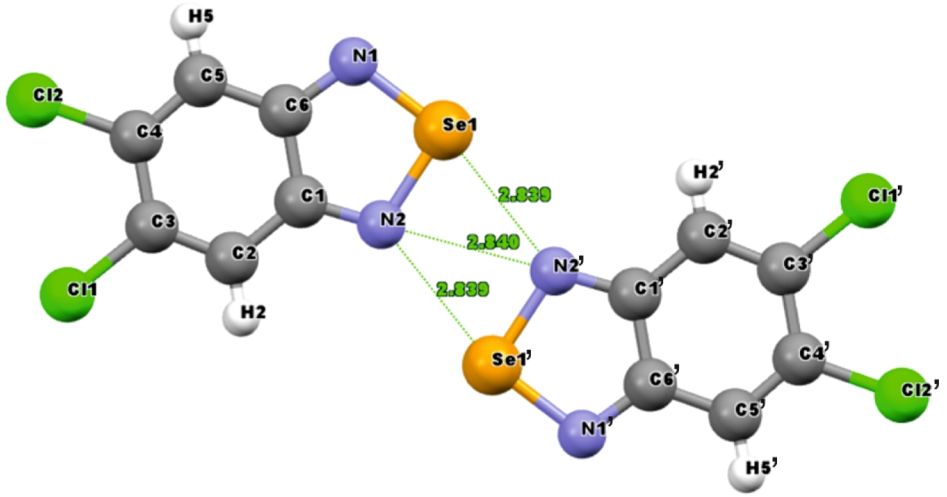

Figure 2. 5,6-Dichloro-2,1,3-benzoselenadiazole dimer stabilized by noncovalent interactions. Interatomic distances are given in Å.

directionality, chalcogen bonding is particularly important in crystal engineering and self-assembly of supramolecular structures. Evidence of chalcogen bond-like motifs in crystalline structures is frequently seen in the literature.[19,34,46−65] An often repeated example is the structure of Ebselen, an essential biological compound, which is stabilized by short Se···O noncovalent contacts.[34] Selenocyanate crystals have recently come under intense investigation[60,65,66] as the substitution of the cyano group strongly enhances one of the σ-holes over the other on the Se atom.[66] Such a strategy extends the possible geometries of emerging crystals beyond the basic "amphoteric" symmetric molecules.[66] Additionally, it has been found that these systems have potential biological activities as, for example, receptors mediating the signal in human prostate cancer cells.[67] In the work of Romito et al.,[68] the functionalized bithiophenes of tunable photophysical properties were successfully synthesized, wherein the use of chalcogen atoms facilitated control of the synthetic pathway.[68] Also, very recently, the Okuniewski group revealed charge-assisted S···S chalcogen contacts in 4,6-dimethyl-2-pyrimido(thio)nium halides.[58]

There are a number of unresolved questions concerning chalcogen bonds. How might the bond be weakened if the electron-donating base is involved not only in the chalcogen bond but is serving simultaneously as a donor in a second noncovalent interaction? While there is some information concerning the cooperativity if these two interactions occur on two different sites within the base, the question has been largely ignored with respect to a single atom serving as a donor in two simultaneous bonds. The issue becomes further complicated if both interactions compete for the same lone electron pair of that atom. A second matter of some importance concerns the presence of two chalcogen bonds within a dimer such that each monomer serves as both the electron donor and acceptor. Due to the symmetry of the system, charge is transferred in both directions and in equal amounts so that the net transfer must be zero. But how does

https://dx.doi.org/10.1021/acs.jpca.0c10814
J. Phys. Chem. A 2021, 125, 657−668

the presence of the second chalcogen bond affect the amount of charge that can be transferred within the first and vice versa?

The current study attempts to answer these questions utilizing a uniquely designed system. 5,6-Dichloro-2,1,3-benzoselenadiazole $C_6H_2Cl_2N_2Se$ (Figure 1) contains a 1,2-Cl phenyl ring, fused to a five-membered selenadiazole ring, with its two N atoms adjacent to the central Se. As such, its homodimer (Figure 2) is likely to contain a pair of Se···N chalcogen bonds, each involving a different pair of Se and N atoms, but the proximity of the two N atoms is close enough that they may also interact with one another in the context of a N···N pnicogen bond which itself has precedent in the literature.[69−76] In the first phase of the work described below, the homodimer in Figure 2 is characterized using various experimental procedures, such as Fourier transform infrared (FT-IR), Raman, and ^{13}C and ^{1}H NMR spectroscopy, as well as an accurate structure determination via X-ray diffraction analysis. This set of data confirms the expectation of the aforementioned Se···N and N···N contacts. As such, this dimer presents a unique opportunity to scrutinize not only the fundamental nature of each noncovalent bond but also the manner in which these interactions affect one another. It should be underscored that the N···N dipnicogen bond has appeared only very rarely in the literature, and this dimer offers the possibility of further detailed study.

In order to acquire a fundamental understanding of the forces involved, quantum chemical calculations are applied to this system as well as to the analogues in which Se is replaced by other chalcogen atoms S and Te. Further probing of the detailed origins of the attractive forces is derived from calculations of derivatives in which (a) one of the N atoms of each monomer is replaced by CH and (b) the entire phenyl ring is removed, along with its Cl substituents.

2. SYNTHESIS

2.1. Preparation of 5,6-Dichloro-2,1,3-benzoselenadiazole ($C_6H_2Cl_2N_2Se$). $SeCl_4$ and 4,5-dichloro-*o*-phenylenediamine were purchased from Sigma-Aldrich and solvents from Avantor (POCH S.A.). All reagents were used without further purification. $SeCl_4$ (0.5 mmol, 0.1104 g) was dissolved in 3 mL of methanol and stirred for 15 min at room temperature. To the stirred mixture, 4,5-dichloro-*o*-phenylenediamine (0.0885 g, 0.500 mmol) dissolved in 2 mL of methanol before was added. Immediately after addition, a fine greyish precipitate appeared, and the stirring was continued for another 60 min. The resulting greyish precipitate was collected by filtration, washed with methanol diethyl ether, and dried in a desiccator for a few days. ^{1}H NMR and ^{13}C NMR spectroscopies were used to check the purity of the new product. Next, the product was dissolved in a dichloromethane and methanol mixture (2:1 ratio) and left to crystallize at room temperature; yellowish crystals appeared after 7 days. [$C_6H_2Cl_2N_2Se$] yield: 0.0895 g, 0.355 mmol (71.0% based on $SeCl_4$).

3. METHODS

3.1. Experimental Methods. The X-ray diffraction data was collected on a Rigaku Oxford Diffraction Supernova Duals Source with an Atlas CCD detector using graphite monochromated Mo Kα radiation (λ = 0.71073 Å) at 100 K. The structure was solved by direct methods using SHELXS and refined by full-matrix least-squares on F^2 using SHELXL-2014.[77] NMR spectra (^{1}H NMR and ^{13}C NMR) were recorded on a Bruker Avance400 MHz with an UltraShield Plus magnet. Chemical shifts (δ) are given in ppm using DMSO-d_6 as the solvent. The vibrational spectral measurements were performed in The Laboratory of Vibrational Spectroscopy belonging to The Faculty of Chemistry at Wroclaw University of Science and Technology. ATR FT-IR spectra of the selenium(IV) complex, $SeCl_4$ and 4,5-dichloro-*o*-phenylenediamine, were collected using a Bruker Vertex 70v Fourier transform infrared spectrophotometer equipped with an air-cooled DTGS detector, gas cell with a temperature controller, and diamond attenuated total reflection infrared cell at 2 cm^{-1} resolution and 64 scans in the middle-infrared (4000−400 cm^{-1}) and far-infrared (600−100 cm^{-1}) regions at room temperature. Instrument control and initial data processing were performed using OPUS software (v. 7.5, Bruker Optics, Ettlingen Germany). The FT-Raman spectra of ligands were collected on a Bruker MultiRam spectrometer (Nd:YAG laser with a CW radiation at 1064 nm) equipped with a liquid N_2 cooled germanium detector at a resolution of 4 cm^{-1}, co-addition of 512 scans, and laser power values of 150 mW for $SeCl_4$, 4,5-dichloro-*o*-phenylenediamine, and selenium complex.

3.2. Computational Methods. Geometry optimization of isolated monomers and dimers was performed at the MP2/aug-cc-pVDZ level of theory.[78−80] The pseudopotential aug-cc-pVDZ-PP[81−85] was used for Te atoms to include relativistic effects. The interaction energy (E_{int}) of each complex refers to the difference in the total electronic energy between the fully optimized complex and the sum of its constituent monomers in the geometry adopted within the complex, while the binding energy (E_b) takes as its reference the monomers in their fully optimized isolated geometries. These two differ by the deformation energies (E_{def}) induced by the complexation process. All energies in this work were corrected by the basis set superposition error via the counterpoise procedure proposed by Boys and Bernardi.[86] Harmonic frequency analysis authenticated that the stationary points on the potential energy surfaces were true minima as imaginary frequencies were absent. Deeper analysis of vibrational modes utilized the potential energy distribution procedure via FCart software. Computational evaluation of ^{1}H NMR chemical shielding used the GIAO approach at the MP2 level. To provide full flexibility to the inner-shell electrons for purposes of NMR calculations, the all-electron Sapporo-DKH3-DZP-2012-diffuse basis set,[87] with relativistic effects included, was used for Te atoms, as a counterpoint to the effective core potential of aug-cc-pVDZ-PP. Calculations made use of the Gaussian 16, C.01 Rev. suite of programs.[88] The QTAIM methodology was used to identify bond paths through analysis of the electron density topology within the AIMAll program.[89] The decomposition of the interaction energies was carried out through the Morokuma−Ziegler scheme (using the ADF software).[90,91] The molecular electrostatic potential (MEP) and its extrema on the 0.001 au electronic isodensity surface of monomers in their fully optimized geometries were assessed via MultiWFN and visualized by VMD programs.[92−94]

3.3. Synthesis and Crystal Structure Characterization. The complex was obtained by adding the ligand 4,5-dichloro-*o*-phenylenediamine to the methanolic solution of $SeCl_4$. Afterward, the compound has been characterized by spectroscopic methods and theoretical calculation. The crystal structure of the selenium complex has been determined by X-

https://dx.doi.org/10.1021/acs.jpca.0c10814
J. Phys. Chem. A 2021, 125, 657−668

ray analysis. The experimental parameters were compared with theoretical values.

4. STRUCTURE DESCRIPTION

The compound obtained by our group 5,6-dichloro-2,1,3-benzoselenadiazole ($C_6H_2Cl_2N_2Se$) crystallizes in the monoclinic $P2_1/c$ space group. The perspective view of its molecular structure together with the atom numbering is shown in Figure 1.

Details of the crystallographic data collection, structural determination, and refinement for 5,6-dichloro-2,1,3-benzoselenadiazole are given in Table S1. The crystal structure has been deposited at the Cambridge Crystallographic Data Centre and allocated to the deposition numbers CCDC 2006282.

The asymmetric unit cell consists of the 4,5-dichloro-*o*-phenylenediamine ligand and selenium(IV) ion and is oriented in one plane; the Se1−N1(1.794(3)) distance is slightly longer than Se1−N2 (1.789(3)) in the same unit. Prima's group[95] obtained the series of 2,1,3-benzoselenadiazoles, that is, the planar molecule 4,5,6,7-tetrachloro-2,1,3-benzoselenadiazole, where they have reported similar Se−N bond distances: 1.792(3) Å and 1.779(3) Å for Se2−N1 and Se2−N3, respectively. The angle N1−Se1−N2 in our selenium(IV) complex is 93.9(1)°, while in 4,5,6,7-tetrachloro-2,1,3-benzoselenadiazole, the N1−Se2−N3 angle is 94.34°.[95]

In Figure 2, the structure of the 5,6-dichloro-2,1,3-benzoselenadiazole dimer is depicted. Four atoms in the Se_2N_2 moiety form a planar quadrilateral. This fact is confirmed by the angles Se1−N2−Se1′ and N2−Se1−N2′ which are 108.3(1) and 71.7(1)°, respectively. The sum of four angles equals 360°. Moreover, these four atoms are located in one plane (dihedral Se1−N2−Se1′−N2′ is 0°). The crystal packing analysis[96] revealed that the 5,6-dichloro-2,1,3-benzoselenadiazole dimer is linked by two chalcogen Se1···N2′ bonds (expl 2.839(3)) supported by one N2···N2′ (expl 2.840 Å) interaction.[97] These distances are shorter than van der Waals contacts (3.48 and 3.32 Å for former and latter, respectively). A similar motif was observed in diselenides and selenocyanates.[98] The Se1···Se1′ distances between two units from the neighboring layers of the complex in the crystal are longer than van der Waals contacts (3.64 Å) ranging between 3.716 and 3.8023(4) Å.

5. SPECTROSCOPIC STUDY

The FT-IR and Raman spectra of the selenium(IV) complex in the middle region are shown in Figure 3. Additionally, the far-infrared region of the absorption complex is shown in Figure 4. The medium bands at 3085 and 3054 cm^{-1} in the FT-IR spectrum of the selenium(IV) compound (5,6-dichloro-2,1,3-benzoselenadiazole) are assigned to ν(C−H) stretching vibrations from two aromatic −CH− groups; in the Raman spectrum, one medium band at 3062 cm^{-1} and one weak band at 3085 cm^{-1} are observed as well. The characteristic stretching modes ν(C−C) in the aromatic ring and ν(C−N) generate the strong intensity bands at 1476 (1481 cm^{-1}, Raman), 1461, 1425 (1427 cm^{-1}, Raman), and 1354 cm^{-1} (1356 cm^{-1}, Raman) in experimental FT-IR spectra of the new complex. The strong peak in the FT-IR spectrum at 1086 cm^{-1}, medium in Raman at 1091 cm^{-1}, can be assigned to the characteristic vibrations, "Star of David", coupled with ν(C−Cl) stretching vibrations. The strong band at 1258 cm^{-1} in the FT-IR spectrum is due to δ(C−H) bending vibrations, which

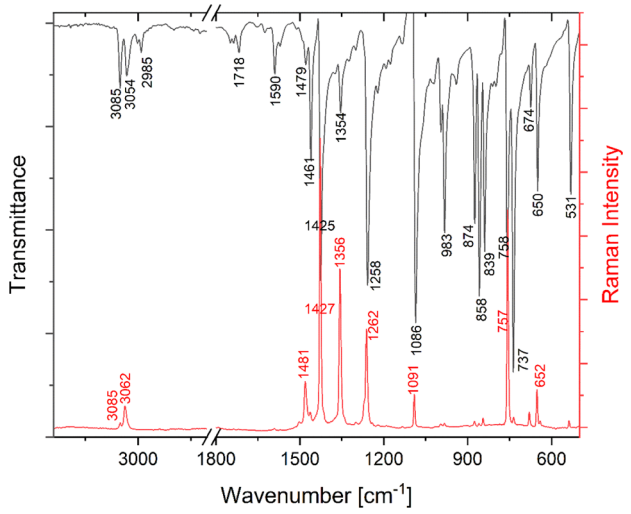

Figure 3. FT-FIR and Raman spectra of the selenium(IV) complex in the range 3400−500 cm^{-1}.

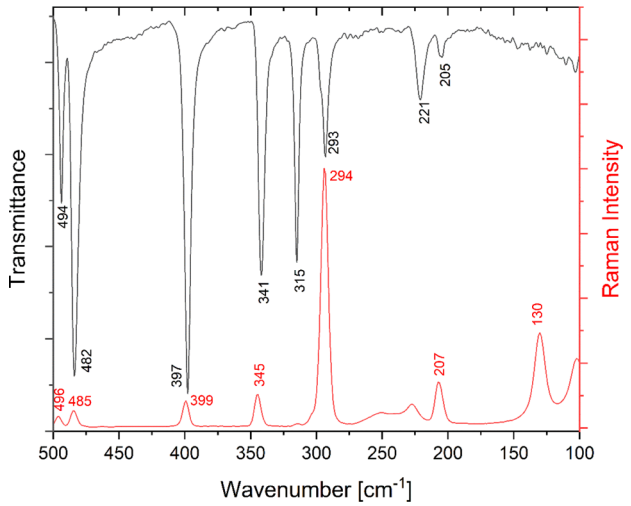

Figure 4. FT-FIR and Raman spectra of the selenium(IV) complex in the range 500−100 cm^{-1}.

correspond to medium at 1262 cm^{-1} in the Raman spectrum of the new complex.

The characteristic "in plane" and "out of plane" bending vibrations involving atoms of the ring generate quite strong bands in the spectral range of 983−650 cm^{-1} in the FT-IR spectrum of the selenium(IV) complex. These modes are coupled with ν(Se−N) stretching and δ(N−Se−N) bending vibrations.[99,100] The two strong bands at 858 and 839 cm^{-1} in the FT-IR spectrum (very weak in the Raman spectrum) are attributed to ν(Se═N).[99,101] Furthermore, the ν(Se···N) stretching vibrations involved in the chalcogen bonds generate the medium band at 531 cm^{-1} in the FT-IR spectrum (not observed in Raman, Figure 4) which confirms the presence of noncovalent interactions that stabilized the structure of the selenium(IV) complex. The characteristic strong band at 341 cm^{-1} (corresponds to medium at 345 cm^{-1} in Raman) and the medium band at 293 cm^{-1} (Raman: 294 cm^{-1}) in the FT-IR spectrum of the selenium(IV) complex are due to the ring deformations coupled with crystal lattice vibrations of the discussed complex.

https://dx.doi.org/10.1021/acs.jpca.0c10814
J. Phys. Chem. A 2021, 125, 657−668

The NMR spectra are shown in the Supporting Information as Figures S1 and S2. The one strong signal at 8.234 ppm in the ^{1}H NMR spectrum is related to the two −CH groups of the phenyl ring which are magnetically equivalent. The ^{1}H NMR chemical shifts of these protons were correlated with the signals at 123.56 ppm in the ^{13}C NMR spectrum. Then, the chemical shifts C1(or C6) and C3(or C4) are 133.599 and 158.122 ppm, respectively. The additional peaks in both NMR spectra that would indicate other than the discussed weak intermolecular interactions are not observed. The peaks in the ^{1}H NMR spectrum of the complex at 2.256 and 3.250 ppm come from the residual DMSO-d_6 and water, respectively; we do not take this into consideration. As a result, the corresponding bands in the FT-IR and Raman spectra supported by signals in NMR spectra of the 5,6-dichloro-2,1,3-benzoselenadiazole confirmed the structure determined by an X-ray analysis.

6. THEORETICAL RESULTS

In order to probe the details of these interactions further, the first set of model systems was homodimers of $C_6H_2Cl_2N_2Y$ (Y = S, Se, and Te). The MEP of one of these monomers, Y═Se, is illustrated in Figure 5 where the most positive and negative

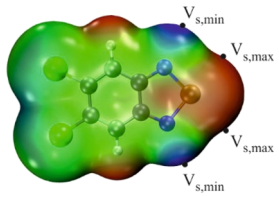

Figure 5. MEP map of the $C_6H_2Cl_2N_2Se$ monomer with extrema indicated on the 0.001 au electron density isosurface (black dots). Color scale from −0.03 (blue) to +0.03 au (red).

regions are indicated in red and blue, respectively. As indicated by the designations in the figure, the minima on the 0.001 au isodensity surface lie approximately along the N lone pairs. The σ-holes, $V_{s,max}$, are situated along the two extensions of the N−Se covalent bonds. The magnitudes of these extrema listed in Table 1 indicate that the intensity of the σ-holes grows steadily along with the size of the Y atom, whereas $V_{s,min}$ is relatively steady.

Table 1. MEP Extrema (kcal/mol) on the 0.001 au Isodensity Surface of the Examined Isolated $C_6H_2Cl_2N_2Ch$ (Ch = S, Se, and Te) Monomers Calculated at the MP2/aug-cc-pVDZ

monomer	$V_{s,max}$	$V_{s,min}$
$C_6H_2Cl_2N_2S$	18.5	−20.0
$C_6H_2Cl_2N_2Se$	25.4	−20.7
$C_6H_2Cl_2N_2Te$	34.2	−22.2

The homodimers of each of these systems form a roughly planar system, as indicated for Y═Se in Figure 6. The two R(Se···N) distances in Table 2 are roughly equal to R(N···N). This near equality persists for the other two systems as well, but it is important to note that these intermolecular separations become progressively shorter even as the radii of the Y atoms grow larger. All of these interatomic distances are shorter than the sum of their vdW radii,[102] suggesting that three noncovalent bonds might be present. The angles displayed in the next columns show first that the C−N···N−C arrangement is very nearly linear. The θ(N2′···Y−N1) angles indicate a roughly linear approach of the N nucleophilic center to the σ-hole generated by the Y−N covalent bond on the ring of the other monomer. This angle is 173° for Y═S but becomes smaller and less linear as Y grows larger.

The last three columns of Table 2 show a rapidly growing binding strength as Y becomes larger. The interaction energy of 5.4 kcal/mol for Y═S is tripled for Te. This trend is in line with previous studies.[34] There is only a small deformation of the monomers as they engage with one another, which leaves E_b only slightly smaller than E_{int}. These small deformations differ from those reported earlier for the set of the YF_4 (Y = S, Se, Te, and Po) complexes with two ammonia ligands, stabilized by two simultaneous Y···N bonds.[103] The deformation energies were substantially larger there, between 18 and 48 kcal/mol, which may be attributed in part to the attack of Lewis bases on both sides of the monomer.

As a check on the validity of the calculations, the optimized geometries may be compared to those within the crystal. Such a comparison is provided in Table 3 for the case of Y═Se. The bond lengths agree within 0.03 Å, and angles are consistent to 1.4°. The intermolecular chalcogen bond lengths are particularly closely mimicked by the calculations.

One can obtain some insights into these interactions by analyzing the wave functions. NBO analysis is provided in Table 4 which provides both atomic charges and an energetic measure of the transfer of charge between individual orbitals. The first three columns of Table 5 show first that the chalcogen atoms are quite positively charged, with $q \sim 1$, and become a bit more so upon forming the complex. The N atoms also intensify their charge, becoming more negative. These changes are especially notable for Y═Te. The next columns provide an energetic measure of each noncovalent bond in terms of the transfer from the N lone pair of one monomer to the indicated antibonding orbital of the other. The σ^*(Y−N1) orbital lies directly opposite the N2 atom so corresponds to the classic chalcogen bonding interaction. This term is the largest of those listed and grows quickly with the Y atomic size, by a factor of 4 from S to Te. This transfer is complemented by a smaller amount into the σ^*(Y−N2) orbital, although this bond is nearly perpendicular to the N2′···Y bonding axis. Another addition arises from what might be described as a N···N pnicogen bond wherein charge is transferred into the C1−N2 antibonding orbital.

An alternate perspective on the bonding arises from AIM analysis of the topography of the electron density.[104−107] The molecular diagrams displayed in Figure S3 all contain a pair of N···Y bond paths. There is also evidence of a N···N bond path for all systems except Y═Te. The absence of this path contradicts the NBO data which would suggest that for Y═Te, the N···N bond is the strongest. The various measures of each noncovalent bond strength are reported in Table 5. The bond critical point (BCP) density in the first column indicates that all bonds grow in strength; both N···N and Y···N strengthen as the Y atom grows in size and as the intermolecular distance shortens. This measure of bond strength indicates that both sorts of bonds are of comparable strength. The Laplacian is positive for all cases, consistent with a noncovalent bond, while H is very nearly equal to 0. The curious absence of a direct N···N bond path in the Te system was checked with a larger all-electron (Sapporo-DKH3-DZP-2012-diffuse) basis set. The

https://dx.doi.org/10.1021/acs.jpca.0c10814
J. Phys. Chem. A 2021, 125, 657−668

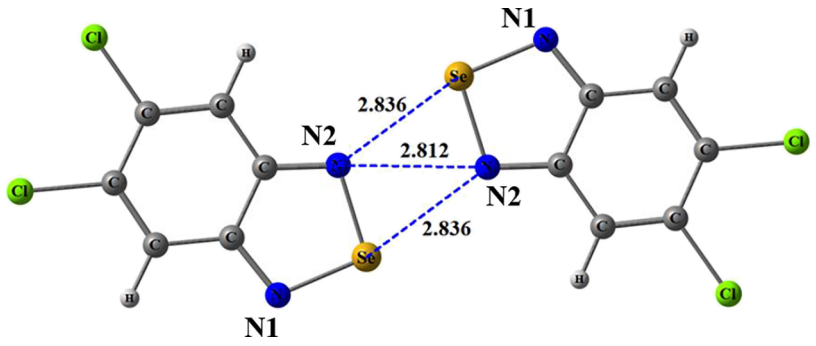

Figure 6. Top and side views of the MP2 optimized structure of the $(C_6H_2Cl_2N_2Se)_2$ homodimer. Distances in Å.

Table 2. Structural and Energetic Parameters of Optimized Homodimers[a]

	r(N2···N2′)	R(Ch···N2′)	θ(C1−N2···N2′)	θ(N2′···Y−N1)	E_{int}	E_b	E_{def}
$C_6H_2Cl_2N_2S$	2.918	2.960	179.9	173.3	−5.39	−5.27	0.12
$C_6H_2Cl_2N_2Se$	2.812	2.836	177.5	166.6	−8.45	−8.13	0.32
$C_6H_2Cl_2N_2Te$	2.674	2.649	174.4	156.7	−16.83	−15.06	1.77

[a]Distances in Å, angles in degs, energies in kcal/mol.

Table 3. Selected Structural Parameters Comparison (Distances in Å, Angles in Degrees) between Theoretical Prediction Made at the MP2/aug-cc-pVDZ Level of Theory and X-ray Structure for the $(C_6H_2Cl_2N_2Se)_2$ Complex

	Theory	Experiment
	Bond distances	
N2−N2′	2.812	2.840
Se1−N2′	2.836	2.839
N2−Se1′	2.836	2.839
C1−N2	1.377	1.328
C1′−N2′	1.377	1.328
N1−Se1	1.795	1.794
N1′−Se1′	1.795	1.794
RMSD[a]	0.030	
	Angles	
C1−N2−N2′	177.5	178.0
C1′−N2′−N2	177.5	178.0
N1−Se1−N2	95.9	93.9
N1′−Se1′−N2′	95.9	93.9
Se1−N2−Se1′	109.3	108.3
N2−Se1−N2′	70.7	71.7
N1−Se1−N2′	166.6	165.4
N1′−Se1′−N2	166.6	165.4
N1−Se1−Se1′	140.2	138.9
N1′−Se1′−Se1	140.2	138.9
RMSD	1.4	

[a]RMSD = root mean square deviation between expt and calculation.

Table 5. BCP Properties: Electron Density ρ, Laplacian of Electron Density $\nabla^2\rho$ and Total Electron Energy H, Obtained at the MP2/aug-cc-pVDZ Level[a]

complex	interaction	ρ	$\nabla^2\rho$	H
$C_6H_2Cl_2N_2S$	N···N	0.013	0.045	0.001
	S···N	0.014	0.046	0.001
$C_6H_2Cl_2N_2Se$	N···N	0.016	0.061	0.001
	Se···N	0.020	0.060	0.001
$C_6H_2Cl_2N_2Te$	Te···N	0.033	0.081	−0.003

[a]Data in au.

results were the same but there was a bit larger value of ρ_{BCP} for the two chalcogen bonds, growing from 0.035 to 0.052 au.

A variant of the AIM formalism is the noncovalent index (NCI) approach which focuses on the reduced density gradient.[3,108,109] The deviation from a homogeneous electron distribution can be transformed into isosurfaces of desired color in accordance with the sign of this change. The green regions lying along the Y···N axes in Figure S4 for S and Se offer additional confirmation of the presence of the chalcogen bonds. Their color change to blue for Te is consistent with a stronger Te···N YB. With respect to the N···N axis, there is a more intensely red area for Te, which bolsters the failure of AIM to visualize a N···N pnicogen bond.

Another means of understanding the forces involved derives from a decomposition of each total interaction energy into its various components. The results of such a deconstruction are contained in Table 6 where the Pauli repulsion is opposed by the three principal attractive components electrostatic, orbital

Table 4. NBO Atomic Charges on Selected Atoms and $E(2)$ Interorbital Transfer Energies of Dimers at the DFT Level of Theory

	atomic charges, e			$E(2)$ from N2 lone pair, kcal/mol[a]		
	Y	N2	N1	σ^*(Y−N1)	σ^*(Y−N2)	σ^*(C1−N2)
$C_6H_2Cl_2N_2S$	0.925 (+0.039)[b]	−0.593 (−0.033)	−0.562 (−0.002)	1.72		0.47
$C_6H_2Cl_2N_2Se$	1.028 (+0.071)	−0.648 (−0.062)	−0.595 (−0.009)	3.60	0.22	0.76
$C_6H_2Cl_2N_2Te$	1.236 (+0.113)	−0.768 (−0.114)	−0.672 (−0.018)	7.51	3.02	1.23

[a]Two such interactions in each case, one in each direction. [b]Change upon complexation.

https://dx.doi.org/10.1021/acs.jpca.0c10814
J. Phys. Chem. A 2021, 125, 657−668

Table 6. Decomposition of Energy Calculated for $C_6H_2Cl_2N_2Y$ Homodimers at the BLYP-D3/ZORA/TZ2P Level

dimers	E_{int}	E_{Pauli}	E_{elec}	%	E_{orb}	%	E_{disp}	%
$C_6H_2Cl_2N_2S$	−3.33	15.97	−10.97	57	−4.83	25	−3.50	18
$C_6H_2Cl_2N_2Se$	−6.26	28.93	−20.27	58	−10.58	30	−4.34	12
$C_6H_2Cl_2N_2Te$	−13.72	78.31	−53.60	58	−32.94	36	−5.49	6

interactions, and dispersion. Each of these terms increases quickly in the order S < Se < Te, particularly E_{elec} and E_{orb}. The former quantity is increased five-fold upon changing from S to Te, for example. Also contained in the table is the percent contribution of each of these attractive terms to their total. It is clear that regardless of the Y atom, the electrostatic component accounts for a constant 58% of the total. The orbital interaction percentage rises with the larger size of Y, while the dispersion changes in the opposite direction. That is, while the dispersion energy itself does rise slowly with larger Y, it does so rather slowly, such that its percentage contribution diminishes from 18% for S down to only 6% for Te.

The chemical shielding of each atom and how it is affected by the complexation offers certain insights into the nature of the bonding as well as provides a bridge to experimental inquiry. The manner in which the shielding of each of the relevant atoms is altered by dimerization is detailed in Table 7.

Table 7. Changes of NMR chemical Shielding (ppm) Caused by Complexation Calculated at the MP2 Level

dimers	Y[a]	N2	N1	C1
$C_6H_2Cl_2N_2S$	−13.5	−10.3	+4.8	+0.9
$C_6H_2Cl_2N_2Se$	−30.0	−21.7	+15.9	+2.5
$C_6H_2Cl_2N_2Te$	−6.9	−54.5	+49.3	+6.4

[a]Average of two Y atoms.

The chalcogen atom suffers a loss of shielding of some 7−30 ppm as indicated in the first column. The N2 atom to which each Y is bonded on the partner monomer, and which is engaged in a pnicogen bond, also undergoes a drop in shielding, which varies from 10.3 ppm for Y═S to as much as 54.5 ppm for Te. The opposite trend of a shielding increase occurs on the other N1 atom, not directly involved in the interactions. Lastly, the C1 atom bonded to N2 which is in turn involved in all intermolecular bonds and is the beneficiary of a small shielding increase, which rises from 0.9 ppm for S up to 6.4 ppm for Te. As can be seen from Table 7, the magnitudes of the chemical shielding for the N and C atoms follow the periodic trend while those for Y do not, what probably could be explained as the consequence of applying different basis sets for Te than in the case of the remaining atoms.

6.1. Other Derivatives. The presence of the electron-withdrawing N1 atom on each monomer is likely responsible for intensification of the σ-hole on each Y atom that attracts a nucleophile. Replacement of N1 by a CH group should logically weaken the σ-hole and the strength of each chalcogen bond. The effects of this substitution on the MEP extrema are listed in the first two columns of Table 8.

Comparison with the corresponding values in Table 1 indeed reflect the anticipated drop in $V_{s,max}$ by nearly 10 kcal/mol. On the other hand, this same replacement intensifies $V_{s,min}$ by nearly 5 kcal/mol. There is thus a certain degree of compensation such that the interaction energies of the complexes of the sort illustrated in Figure 7 decline by a

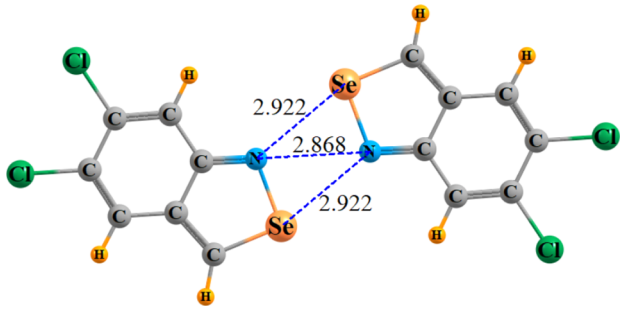

Figure 7. MP2 optimized structure of the $(C_7H_3Cl_2NSe)_2$ homodimer. Distances in Å.

relatively small amount, between 12 and 22%. Intermolecular distances undergo small elongations as well. The internitrogen distance stretches by 0.02−0.08 Å, as does R(Y···N) by 0.05−0.11 Å. Another piece of evidence of somewhat weakened noncovalent bonds is the reduction in the bond critical point densities of both the N···N and Y···N interactions, which remain comparable to one another but are lower than their values in the unsubstituted dimers by 15−25%. The NBO analysis provides a slightly different picture. Despite its lengthening, the chalcogen bond $E(2)$ quantities are a bit larger in the substituted systems, whereas the N···N pnicogen bonds are considerably weaker, with all $E(2)$ values reduced by a factor of 1/3.

Another variation would be to remove the second phenyl ring, along with its Cl substituents, leaving a single $C_2N_2H_2Y$ ring, as illustrated in Figure 8 for Y═Se. Like the N → CH substitution, this ring removal also reduces $V_{s,min}$ while simultaneously enhancing $V_{s,max}$, as documented in Table 9.

The effect on the interaction energy is quite similar to that caused by the earlier substitution, although the intermolecular distances are a bit shorter when the ring is removed. AIM measures of both chalcogen and pnicogen bonds are quite similar in both cases, as are the NBO quantities, although NBO does indicate slightly stronger bonds as a result of ring removal as compared to N → CH replacement. Altogether, it would

Table 8. Computed Properties of Homodimers with N replaced by CH in Each Monomer

	$V_{s,max}$ (kcal/mol)	$V_{s,min}$ (kcal/mol)	E_{int} (kcal/mol)	R(N···N) (Å)	R(Y···N) (Å)	ρ(N···N) (au)	ρ(Y···N) (au)	$E(2)$ N′ → YC (kcal/mol)	$E(2)$ N′ → NC (kcal/mol)
$C_7H_3Cl_2NS$	10.6	−25.2	−4.76	2.942	3.006	0.011	0.012	2.09	0.14
$C_7H_3Cl_2NSe$	16.7	−25.3	−7.12	2.868	2.922	0.013	0.015	4.58	0.23
$C_7H_3Cl_2NTe$	25.2	−25.9	−13.09	2.752	2.763		0.026	10.77	0.40

https://dx.doi.org/10.1021/acs.jpca.0c10814
J. Phys. Chem. A 2021, 125, 657−668

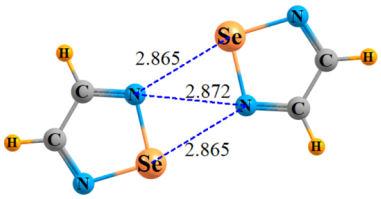

Figure 8. MP2 optimized structure of the $(C_2N_2H_2Se)_2$ homodimer. Distances in Å.

appear that either sort of modification weakens the interaction, although the effects of ring removal are a bit less severe than substitution of N by CH. The effect of a N atom within a ring of this sort to enhance the σ-hole and thus the strength of a nearby chalcogen bond has been observed before[110] in the context of a bidentate interaction with an anionic nucleophile.

7. DISCUSSION

It is instructive to place the results obtained in this work in the broader context of earlier projects. In terms of examination of NMR aspects of chalcogen bonded complexes, our group considered previously the HFY complexes (Y = S, Se, and Te) with *N*-methylacetamide.[111] NMR chemical shifts caused by complexation had an opposite sign (increase from 141.2 to 1310.8 ppm) and significantly greater magnitude than those computed in the current work. Also, despite using the same basis set, the pattern of this change with respect to the Y atoms was not preserved. This observation is linked with the atomic charge perturbations upon complexation which offers a point of consistency. In the cited work, a drop in atomic charge contrasts with the gain here. These differences help explain different directions of NMR shifts with the reasonable presumption that shielding of each atom is related to the total electron density which surrounds the nucleus. With regard to the interaction energies of Y···N chalcogen bonds, they range between −8.90 and −13.82 kcal/mol in the earlier work, similar to the current systems, and present the same trend: this quantity escalates along with the size of the Y atom, so it is largest for the Te-containing dimers.

Effects on the NMR spectra induced by chalcogen bonding were also examined in an earlier work where FHY complexes (Y = S, Se, and Te) with ammonia were investigated.[112] For the S and Se atoms, the intensification of chemical shielding that accompanies dimerization was 264 and 848 ppm, respectively, while for the Te atom, it dramatically dropped to only 35 ppm. Again, the rising of Y atom shielding was consistent with the falling of the corresponding atomic charge. Interaction energies of complexes evaluated here were in a similar range and obeyed a similar pattern as in the current work (from about −9 to −16 kcal/mol, in line with the boost of the chalcogen atomic radius). Another approach to the chalcogen bond properties was made for a set of trimers between two ammonia molecules and YF_4 (Y = S, Se, Te, and Po).[103] Complexes were more strongly bound (with E_{int} even more than −50 kcal/mol) but still undergo the same systematic tendency connected with the chalcogen atom size (observed for cis type complexes), such as the growth in the stability of complexes from S to those with Po atoms (−13 to −37 kcal/mol). The main difference between these two series of results was the impact of the deformation energy. In the case of our current work, the deformation plays a minor role (not exceeding 2 kcal/mol) while in the abovementioned work,[103] it was a huge factor in the complexation process contributing up to 50 kcal/mole. The contribution of geometry distortion in chalcogen bonded systems has been reported elsewhere[113,114] as well as the importance of the chalcogen atom size (or substituent impact) for the overall stability of chalcogen bonded complexes.[114−118]

The alignment of the two Se···N chalcogen bonds facilitates the flow of electrons in both directions at once, in the sense that each monomer acts simultaneously as both the electron donor and acceptor. In an effort to assess the potential cooperative effects of such an arrangement, one of the molecules in Figure 8 was rotated around the Se···N intermolecular axis, such that the dihedral angle φ(NSe···NSe) = 90°, thereby breaking the other Se···N chalcogen bonds. The counterpoise-corrected interaction energy dropped from 7.11 to 2.74 kcal/mol as a result of this reorientation. Part of this energy loss arises from the removal of the N···N interaction for which there is no bond path in the perpendicular arrangement. Another factor is the weakening of the remaining Se···N chalcogen bond which sees its $E(2)$ perturbation energy diminish from 6.26 to 5.77 kcal/mol. So there is some evidence of a positive cooperativity associated with the symmetric pairing of the two Se···N bonds in the coplanar dimer. There is moreover reason to believe that the symmetric N···N dipnicogen bond constitutes a second factor that amplifies the overall interaction.

Interplay between noncovalent interactions in this work involves the relationship between chalcogen and pnicogen bonds. In previous literature reports, one can find some insights into the cooperativity of the chalcogen bond. One example arises in the study of F_2CX (X = Se and Te) trimers with NCH or ammonia.[119] It was exhibited that there is an anti-cooperativity effect between chalcogen and tetrel bonds—interaction energies of the former decrease in the presence of the latter and vice versa. The work of Esrafili et al.[120] sheds some further light on the cooperativity effects in systems including a chalcogen bond. It has been shown that in NCH···OCX_n and NCLi···OCX_n (X = S, Se; n = 2−5) linear clusters, the hydrogen- or lithium bonds strengthen and shorten chalcogen bonds in comparison to the bare chalcogen bonded dyads. The same group also demonstrated that a chalcogen bond can cooperate with an aerogen bond in the Y···SHCN···XO_3 triads (Y = NH_3, N_2; X = Ar, Kr).[121] It was also shown that the cooperative energies (oscillating around −0.5 to −1 kcal/mol) depend on the solvent polarity in the order: water > DMSO > acetone. Recently, the cooperation between chalcogen and alkaline-earth bonds was reported for MCl_2···

Table 9. Computed Properties of Homodimers with the Secondary Phenyl Ring Removed

	$V_{s,max}$ (kcal/mol)	$V_{s,min}$ (kcal/mol)	E_{int} (kcal/mol)	R(N···N) (Å)	R(Y···N) (Å)	ρ(N···N) (au)	ρ(Y···N) (au)	$E(2)$ N2′ → YN1 (kcal/mol)	$E(2)$ N2′ → N1C (kcal/mol)
$C_2H_2N_2S$	12.9	−25.2	−4.36	2.983	3.000	0.010	0.011	2.50	0.15
$C_2H_2N_2Se$	19.1	−25.9	−7.11	2.872	2.865	0.013	0.017	6.29	0.26
$C_2H_2N_2Te$	27.9	−27.1	−15.85	2.666	2.589		0.035	19.33	0.58

https://dx.doi.org/10.1021/acs.jpca.0c10814
J. Phys. Chem. A 2021, 125, 657−668

$X_2Y\cdots$N-base (M = Be, Mg; Y = S, Se; X = F, Cl; N-base = NH_3, CH_2 = NH, HCN) ternary clusters.[122] The attachment of the alkaline metal donor group improves the binding enthalpy of the chalcogen bonded binary complex up to a factor of five.

Relatively rarely explored in computational studies is the topic of the N···N dipnicogen interaction. Reyma and Suresh scrutinized nitrogen···nitrogen (as well as C···C and O···O) interactions in homogeneous dimers of organic dipolar molecules.[69] The interaction between these two electronegative centers was explained by means of local polarization which resulted in the appearance of the electron-rich and electron-deficient regions on the surface of two identical monomers. The interaction energies of the dimers increased with an increasing dipole moment of each monomer, reaching up to −8.69 kcal/mol for the methyl cyanate dimer. The N···N interatomic distances were in the range of 3.2 to 3.7 Å, thus considerably longer than in the current work. It must be stressed that in the systems discussed by these authors, numerous hydrogen bond-type contacts supported stabilization of the dimers.

8. CONCLUSIONS

The title systems are held together by a set of noncovalent bonds. Four atoms in the Se_2N_2 moiety form a quadrilateral, as confirmed by the X-ray data. There is first a pair of Y···N chalcogen bonds, with the charge transferring from N to Y in both bonds simultaneously, and in equal amounts, so that there is no net transfer between monomers. This concomitant electron transfer in both directions serves to enhance the binding in a cooperative fashion. The crystal packing analysis shows that the 5,6-dichloro-2,1,3-benzoselenadiazole dimer is linked by two chalcogen Se1···N2′ bonds supported by one N2···N2′ interaction. There is also a N···N pnicogen bond of roughly equal length to the two chalcogen bonds and which appears to be of comparable strength. This interaction appears to be rather strong despite the fact that the lone electron pair on each N atom must contribute to the charge transfer of a neighboring chalcogen bond as well. Additionally, the ν(Se···N) stretching vibrations involved in the chalcogen bonds generate a medium band at 531 cm^{-1} in the FT-IR spectrum which confirms the presence of noncovalent interactions stabilizing the structure of the selenium(IV) complex. The total interaction energy of these homodimers, encompassing all three bonds, covers a wide range from 5.4 kcal/mol for Y═S up to 16.8 kcal/mol for the larger Te. Replacement of one of the N atoms of the 5-membered diazole ring by CH causes a mild weakening of the interaction, due in part to the attenuation of the σ-holes located on the chalcogen atoms. Rather similar effects arise when the dichlorosubstituted phenyl ring is removed, leaving behind the bare diazole ring.

■ ASSOCIATED CONTENT

Supporting Information

The Supporting Information is available free of charge at https://pubs.acs.org/doi/10.1021/acs.jpca.0c10814.

NMR spectra; crystal data; AIM diagrams; NCI diagrams; and coordinates of systems studied (PDF)

■ AUTHOR INFORMATION

Corresponding Authors

Mariusz Michalczyk − *Faculty of Chemistry, Wroclaw University of Science and Technology, 50-370 Wroclaw, Poland;* orcid.org/0000-0002-6495-6963; Email: mariusz.michalczyk@pwr.edu.pl

Magdalena Malik − *Faculty of Chemistry, Wroclaw University of Science and Technology, 50-370 Wroclaw, Poland;* Email: magdalena.malik@pwr.edu.pl

Authors

Wiktor Zierkiewicz − *Faculty of Chemistry, Wroclaw University of Science and Technology, 50-370 Wroclaw, Poland;* orcid.org/0000-0002-4038-5959

Steve Scheiner − *Department of Chemistry and Biochemistry, Utah State University Logan, Logan, Utah 84322-0300, United States;* orcid.org/0000-0003-0793-0369

Complete contact information is available at: https://pubs.acs.org/10.1021/acs.jpca.0c10814

Notes

The authors declare no competing financial interest.

■ ACKNOWLEDGMENTS

This work was financed in part by a statutory activity subsidy from the Polish Ministry of Science and Higher Education for the Faculty of Chemistry of Wroclaw University of Science and Technology. A generous computer time from the Wroclaw Supercomputer and Networking Center is acknowledged. This material is based upon work supported by the National Science Foundation under grant no. 1954310.

■ REFERENCES

(1) Alkorta, I.; Elguero, J.; Frontera, A. Not Only Hydrogen Bonds: Other Noncovalent Interactions. *Crystals* **2020**, *10*, l80.

(2) Clark, T.; Murray, J. S.; Politzer, P. A perspective on quantum mechanics and chemical concepts in describing noncovalent interactions. *Phys. Chem. Chem. Phys.* **2018**, *20*, 30076−30082.

(3) Johnson, E. R.; Keinan, S.; Mori-Sánchez, P.; Contreras-García, J.; Cohen, A. J.; Yang, W. Revealing Noncovalent Interactions. *J. Am. Chem. Soc.* **2010**, *132*, 6498−6506.

(4) Liu, Y.-Z.; Yuan, K.; Liu, L.; Yuan, Z.; Zhu, Y.-C. Anion Recognition Based on a Combination of Double-Dentate Hydrogen Bond and Double-Side Anion−π Noncovalent Interactions. *J. Phys. Chem. A* **2017**, *121*, 892−900.

(5) Müller-Dethlefs, K.; Hobza, P. Noncovalent Interactions: A Challenge for Experiment and Theory. *Chem. Rev.* **2000**, *100*, 143−168.

(6) Strekowski, L.; Wilson, B. Noncovalent interactions with DNA: An overview. *Mutat. Res., Fundam. Mol. Mech. Mutagen.* **2007**, *623*, 3−13.

(7) Riley, K. E.; Hobza, P. Noncovalent interactions in biochemistry. *Wiley Interdiscip. Rev. Comput. Mol. Sci.* **2011**, *1*, 3−17.

(8) *Non-covalent Interactions in the Synthesis and Design of New Compounds*; Maharramov, A. M., Mahmudov, K. T., Kopylovich, M. N., Pombeiro, A. J. L., Eds.; John Wiley & Sons, Inc.: Hoboken, 2016.

(9) Breugst, M.; Koenig, J. J. sigma-Hole Interactions in Catalysis. *Eur. J. Org. Chem.* **2020**, 5473−5487.

(10) Desiraju, G. R.; Steiner, T. *The Weak Hydrogen Bond: In Structural Chemistry and Biology*; International Union of Crystallography, 2006.

(11) Politzer, P.; Murray, J. S. Analysis of Halogen and Other sigma-Hole Bonds in Crystals. *Crystals* **2018**, *8*, 42.

(12) Benz, S.; Poblador-Bahamonde, A. I.; Low-Ders, N.; Matile, S. Catalysis with Pnictogen, Chalcogen, and Halogen Bonds. *Angew. Chem., Int. Ed.* **2018**, *57*, 5408−5412.
(13) Fanfrlík, J.; Zierkiewicz, W.; Svec, P.; Ruzickova, Z.; Rezac, J.; Michalczyk, M.; Ruzicka, A.; Michalska, D.; Hobza, P. Pnictogen bonding in pyrazine*PnX5 (Pn = P, As, Sb and X = F, Cl, Br) complexes. *J. Mol. Model.* **2017**, *23*, 328.
(14) Afkhami, F. A.; Mahmoudi, G.; Qu, F. R.; Gupta, A.; Kose, M.; Zangrando, E.; Zubkov, F. I.; Alkorta, I.; Safin, D. A. Supramolecular lead(II) architectures engineered by tetrel bonds. *Crystengcomm* **2020**, *22*, 2389−2396.
(15) Daolio, A.; Scilabra, P.; Terraneo, G.; Resnati, G. C(sp(3)) atoms as tetrel bond donors: A crystallographic survey. *Coord. Chem. Rev.* **2020**, *413*, 213265.
(16) Franconetti, A.; Frontera, A. Theoretical and Crystallographic Study of Lead(IV) Tetrel Bonding Interactions. *Chem.—Eur. J.* **2019**, *25*, 6007−6013.
(17) Murray, J. S.; Politzer, P. sigma-Holes and Si...N intramolecular interactions. *J. Mol. Model.* **2019**, *25*, 101.
(18) Roeleveld, J. J.; Lekanne Deprez, S. J.; Verhoofstad, A.; Frontera, A.; Vlugt, J. I.; Mooibroek, T. J. Engineering Crystals Using sp 3 -C Centred Tetrel Bonding Interactions. *Chemistry* **2020**, *26*, 10126−10132.
(19) Resnati, G.; Scilabra, P.; Terraneo, G. Chalcogen Bonding in Crystal Engineering. *Acta Crystallogr., Sect. A: Found. Adv.* **2019**, *75*, No. E488.
(20) Murray, J. S.; Resnati, G.; Politzer, P. Close contacts and noncovalent interactions in crystals. *Faraday Discuss.* **2017**, *203*, 113−130.
(21) Arunan, E.; Desiraju, G. R.; Klein, R. A.; Sadlej, J.; Scheiner, S.; Alkorta, I.; Clary, D. C.; Crabtree, R. H.; Dannenberg, J. J.; Hobza, P.; et al. Definition of the hydrogen bond (IUPAC Recommendations 2011). *Pure Appl. Chem.* **2011**, *83*, 1637−1641.
(22) Desiraju, G. R.; Steiner, T. *The Weak Hydrogen Bond: In Structural Chemistry and Biology*. International Union of Crystal, 2001; Vol. *9*.
(23) Espinosa, E.; Mata, I.; Alkorta, I.; Molins, E. Molecular structure and properties: Looking at hydrogen bonds. *Acta Crystallogr., Sect. A: Found. Adv.* **2007**, *63*, S37.
(24) Grabowski, S. J. *Hydrogen Bonding—New Insights*; Springer: Berlin, 2006; Vol. *3*.
(25) Grabowski, S. J. What is the covalency of hydrogen bonding? *Chem. Rev.* **2011**, *111*, 2597−2625.
(26) Scheiner, S. The Hydrogen Bond: A Hundred Years and Counting. *J. Indian Inst. Sci.* **2020**, *100*, 61−76.
(27) Bauzá, A.; Mooibroek, T. J.; Frontera, A. The Bright Future of Unconventional σ/π-Hole Interactions. *Chemphyschem* **2015**, *16*, 2496−2517.
(28) Politzer, P.; Murray, J. S. sigma-Hole Interactions: Perspectives and Misconceptions. *Crystals* **2017**, *7*, 212.
(29) Politzer, P.; Murray, J. S.; Clark, T.; Resnati, G. The σ-hole revisited. *Phys. Chem. Chem. Phys.* **2017**, *19*, 32166−32178.
(30) Clark, T.; Hennemann, M.; Murray, J. S.; Politzer, P. Halogen bonding: the σ-hole. *J. Mol. Model.* **2007**, *13*, 291−296.
(31) Murray, J. S.; Lane, P.; Politzer, P. A predicted new type of directional noncovalent interaction. *Int. J. Quantum Chem.* **2007**, *107*, 2286−2292.
(32) Politzer, P.; Lane, P.; Concha, M. C.; Ma, Y.; Murray, J. S. An overview of halogen bonding. *J. Mol. Model.* **2007**, *13*, 305−311.
(33) Murray, J. S.; Lane, P.; Politzer, P. Expansion of the σ-hole concept. *J. Mol. Model.* **2009**, *15*, 723−729.
(34) Vogel, L.; Wonner, P.; Huber, S. M. Chalcogen Bonding: An Overview. *Angew. Chem., Int. Ed.* **2019**, *58*, 1880−1891.
(35) Bauzá, A.; Mooibroek, T. J.; Frontera, A. sigma-Hole Opposite to a Lone Pair: Unconventional Pnicogen Bonding Interactions between ZF(3) (Z=N, P, As, and Sb) Compounds and Several Donors. *Chemphyschem* **2016**, *17*, 1608−1614.
(36) Solel, E.; Kozuch, S. On the Power of Geometry over Tetrel Bonds. *Molecules* **2018**, *23*, 2742.
(37) Grabowski, S. J. The Nature of Triel Bonds, a Case of B and Al Centres Bonded with Electron Rich Sites. *Molecules* **2020**, *25*, 2703.
(38) Bauzá, A.; Frontera, A. Aerogen Bonding Interaction: A New Supramolecular Force? *Angew. Chem., Int. Ed.* **2015**, *54*, 7340−7343.
(39) Wang, W.; Ji, B.; Zhang, Y. Chalcogen bond: A sister noncovalent bond to halogen bond. *J. Phys. Chem. A* **2009**, *113*, 8132−8135.
(40) Aakeroy, C. B.; Bryce, D. L.; Desiraju, G. R.; Frontera, A.; Legon, A. C.; Nicotra, F.; Rissanen, K.; Scheiner, S.; Terraneo, G.; Metrangolo, P.; et al. Definition of the chalcogen bond (IUPAC Recommendations 2019). *Pure Appl. Chem.* **2019**, *91*, 1889−1892.
(41) Wang, W.; Zhu, H.; Liu, S.; Zhao, Z.; Zhang, L.; Hao, J.; Wang, Y. Chalcogen-Chalcogen Bonding Catalysis Enables Assembly of Discrete Molecules. *J. Am. Chem. Soc.* **2019**, *141*, 9175−9179.
(42) Ho, P. C.; Wang, J. Z.; Meloni, F.; Vargas-Baca, I. Chalcogen bonding in materials chemistry. *Coord. Chem. Rev.* **2020**, *422*, 213464.
(43) Mahmudov, K. T.; Kopylovich, M. N.; Guedes da Silva, M. F. C.; Pombeiro, A. J. L. Chalcogen bonding in synthesis, catalysis and design of materials. *Dalton Trans.* **2017**, *46*, 10121−10138.
(44) Newberry, R. W.; Raines, R. T. Secondary Forces in Protein Folding. *ACS Chem. Biol.* **2019**, *14*, 1677−1686.
(45) Taylor, M. S. Anion recognition based on halogen, chalcogen, pnictogen and tetrel bonding. *Coord. Chem. Rev.* **2020**, *413*, 213270.
(46) Ams, M. R.; Trapp, N.; Schwab, A.; Milić, J. V.; Diederich, F. Chalcogen Bonding ″2S-2N Squares″ versus Competing Interactions: Exploring the Recognition Properties of Sulfur. *Chem.—Eur. J.* **2019**, *25*, 323−333.
(47) Biot, N.; Bonifazi, D. Concurring Chalcogen- and Halogen-Bonding Interactions in Supramolecular Polymers for Crystal Engineering Applications. *Chem.—Eur. J.* **2020**, *26*, 2904−2913.
(48) Channar, P. A.; Saeed, A.; Larik, F. A.; Flörke, U.; El-Seedi, H.; Rodríguez Pirani, L. S.; Erben, M. F. An intramolecular 1,5-chalcogen bond on the conformational preference of carbonyl thiocarbamate species. *New J. Chem.* **2020**, *44*, 5243−5253.
(49) Fanfrlík, J.; Hnyk, D.; Hobza, P. Chalcogen Bonding due to the Exo-Substitution of Icosahedral Dicarbaborane. *Molecules* **2019**, *24*, 2657.
(50) Fellowes, T.; White, J. M. New insights into chalcogen bonding provided by co-crystal structures of benzisoselenazolinone derivatives and nitrogen bases. *Crystengcomm* **2019**, *21*, 1539−1542.
(51) Gogoi, A.; Nashre-ul-Islam, S. M.; Frontera, A.; Bhattacharyya, M. K. Supramolecular association in Cu(II) and Co(II) coordination complexes of 3,5-dimethylpyrazole: Experimental and theoretical studies. *Inorg. Chim. Acta* **2019**, *484*, 133−141.
(52) Kar, S.; Bairagi, S.; Saha, K.; Raghavendra, B.; Ghosh, S. Chalcogen stabilized trimetallic clusters: synthesis, structures, and bonding of [(Cp*M)3(E)6+m(BH)n] (M = Nb or Ta; E = S or Se; m = 0 or 1 or 2; n = 0 or 1). *Dalton Trans.* **2019**, *48*, 4203−4210.
(53) Kaźmierczak, M.; Katrusiak, A. The shortest chalcogen center dot center dot center dot halogen contacts in molecular crystals. *Acta Crystallogr., Sect. B: Struct. Sci., Cryst. Eng. Mater.* **2019**, *75*, 865−869.
(54) Kinzhalov, M. A.; Popova, E. A.; Petrov, M. L.; Khoroshilova, O. V.; Mahmudov, K. T.; Pombeiro, A. J. L. Pnicogen and chalcogen bonds in cyclometalated iridium(III) complexes. *Inorg. Chim. Acta* **2018**, *477*, 31−33.
(55) Kříž, K.; Fanfrlik, J.; Lepsik, M. Chalcogen Bonding in Protein-Ligand Complexes: PDB Survey and Quantum Mechanical Calculations. *ChemPhysChem* **2018**, *19*, 2540−2548.
(56) Kumar, V.; Xu, Y.; Bryce, D. L. Double Chalcogen Bonds: Crystal Engineering Stratagems via Diffraction and Multinuclear Solid-State Magnetic Resonance Spectroscopy. *Chem.—Eur. J.* **2020**, *26*, 3275−3286.
(57) Lundemba, A. S.; Bibelayi, D. D.; Wood, P. A.; Pradon, J.; Yav, Z. G. σ-Hole interactions in small-molecule compounds containing divalent sulfur groups R 1-S-R 2. *Acta Crystallogr., Sect. B: Struct. Sci., Cryst. Eng. Mater.* **2020**, *76*, 707−718.
(58) Okuniewski, A.; Rosiak, D.; Chojnacki, J. Impact of the anion and chalcogen on the crystal structure and properties of 4,6-dimethyl-

2-pyrimido(thio)nium halides. *Acta Crystallogr., Sect. C: Struct. Chem.* **2020**, *76*, 468.
(59) Pandiyan, B. V.; Deepa, P.; Kolandaivel, P. Studies on the sigma-hole bonds (halogen, chalcogen, pnicogen and carbon bonds) based on the orientation of crystal structure. *Mol. Phys.* **2016**, *114*, 3629−3642.
(60) Riel, A. M. S.; Jeannin, O.; Berryman, O. B.; Fourmigué, M. Co-crystals of an organic triselenocyanate with ditopic Lewis bases: recurrent chalcogen bond interactions motifs. *Acta Crystallogr., Sect. B: Struct. Sci., Cryst. Eng. Mater.* **2019**, *75*, 34−38.
(61) Scilabra, P.; Murray, J. S.; Terraneo, G.; Resnati, G. Chalcogen Bonds in Crystals of Bis(o-anilinium)diselenide Salts. *Cryst. Growth Des.* **2019**, *19*, 1149−1154.
(62) Scilabra, P.; Terraneo, G.; Resnati, G. The Chalcogen Bond in Crystalline Solids: A World Parallel to Halogen Bond. *Acc. Chem. Res.* **2019**, *52*, 1313−1324.
(63) von Grotthuss, E.; Nawa, F.; Bolte, M.; Lerner, H.-W.; Wagner, M. Chalcogen-chalcogen-bond activation by an ambiphilic, doubly reduced organoborane. *Tetrahedron* **2019**, *75*, 26−30.
(64) Walton, I.; Chen, C.; Rimsza, J. M.; Nenoff, T. M.; Walton, K. S. Enhanced Sulfur Dioxide Adsorption in UiO-66 Through Crystal Engineering and Chalcogen Bonding. *Cryst. Growth Des.* **2020**, *20*, 6139−6146.
(65) Wang, H.; Liu, J.; Wang, W. Intermolecular and very strong intramolecular C-Se center dot center dot center dot O/N chalcogen bonds in nitrophenyl selenocyanate crystals. *Phys. Chem. Chem. Phys.* **2018**, *20*, 5227−5234.
(66) Riel, A. M. S.; Huynh, H.-T.; Jeannin, O.; Berryman, O.; Fourmigué, M. Organic Selenocyanates as Halide Receptors: From Chelation to One-Dimensional Systems. *Cryst. Growth Des.* **2019**, *19*, 1418−1425.
(67) Facompre, N. D.; El-Bayoumy, K.; Sun, Y.-W.; Pinto, J. T.; Sinha, R. 1,4-Phenylenebis(Methylene)Selenocyanate, but Not Selenomethionine, Inhibits Androgen Receptor and Akt Signaling in Human Prostate Cancer Cells. *Canc. Prev. Res.* **2010**, *3*, 975−984.
(68) Romito, D.; Biot, N.; Babudri, F.; Bonifazi, D. Non-covalent bridging of bithiophenes through chalcogen bonding grips. *New J. Chem.* **2020**, *44*, 6732−6738.
(69) Remya, K.; Suresh, C. H. Intermolecular carbon-carbon, nitrogen-nitrogen and oxygen-oxygen non-covalent bonding in dipolar molecules. *Phys. Chem. Chem. Phys.* **2015**, *17*, 18380−18392.
(70) Młodzikowska, K.; Rajkiewicz, A. A.; Grela, K.; Trzaskowski, B. Boron-boron, carbon-carbon and nitrogen-nitrogen bonding in N-heterocyclic carbenes and their diazaboryl and triazole analogues: Wanzlick equilibrium revisited. *New J. Chem.* **2018**, *42*, 6183−6190.
(71) Kosobokov, M. D.; Sandleben, A.; Vogt, N.; Klein, A.; Vicic, D. A. Nitrogen-Nitrogen Bond Formation via a Substrate-Bound Anion at a Mononuclear Nickel Platform. *Organometallics* **2018**, *37*, 521−525.
(72) Guo, Q.; Lu, Z. Recent Advances in Nitrogen-Nitrogen Bond Formation. *Synthesis* **2017**, *49*, 3835−3847.
(73) Du, Y.-L.; He, H.-Y.; Higgins, M. A.; Ryan, K. S. A heme-dependent enzyme forms the nitrogen-nitrogen bond in piperazate. *Nat. Chem. Biol.* **2017**, *13*, 836.
(74) Abucayon, E. G.; Powell, D. R.; Richter-Addo, G. B. Carbon-Nitrogen and Nitrogen-Nitrogen Bond Formation from Nucleophilic Attack at Coordinated Nitrosyls in Fe and Ru Heme Models. *J. Am. Chem. Soc.* **2017**, *139*, 9495−9498.
(75) Chaban, V. V.; Prezhdo, O. V. Nitrogen-Nitrogen Bonds Undermine Stability of N-Doped Graphene. *J. Am. Chem. Soc.* **2015**, *137*, 11688−11694.
(76) Blair, L. M.; Sperry, J. Natural Products Containing a Nitrogen-Nitrogen Bond. *J. Nat. Prod.* **2013**, *76*, 794−812.
(77) Sheldrick, G. M. Crystal structure refinement with SHELXL. *Acta Crystallogr., Sect. C: Struct. Chem.* **2015**, *71*, 3−8.
(78) Dunning, T. H. Gaussian-Basis Sets for Use in Correlated Molecular Calculations .1. The Atoms Boron through Neon and Hydrogen. *J. Chem. Phys.* **1989**, *90*, 1007−1023.
(79) Møller, C.; Plesset, M. S. Note on an approximation treatment for many-electron systems. *Phys. Rev.* **1934**, *46*, 0618−0622.
(80) Woon, D. E.; Dunning, T. H. Gaussian basis sets for use in correlated molecular calculations. V. Core-valence basis sets for boron through neon. *J. Chem. Phys.* **1995**, *103*, 4572−4585.
(81) Feller, D. The role of databases in support of computational chemistry calculations. *J. Comput. Chem.* **1996**, *17*, 1571−1586.
(82) Metz, B.; Stoll, H.; Dolg, M. Small-core multiconfiguration-Dirac-Hartree-Fock-adjusted pseudopotentials for post-d main group elements: Application to PbH and PbO. *J. Chem. Phys.* **2000**, *113*, 2563−2569.
(83) Peterson, K. A. Systematically convergent basis sets with relativistic pseudopotentials. I. Correlation consistent basis sets for the post-d group 13-15 elements. *J. Chem. Phys.* **2003**, *119*, 11099−11112.
(84) Pritchard, B. P.; Altarawy, D.; Didier, B.; Gibson, T. D.; Windus, T. L. A New Basis Set Exchange: An Open, Up-to-date Resource for the Molecular Sciences Community. *J. Chem. Inf. Model.* **2019**, *59*, 4814−4820.
(85) Schuchardt, K. L.; Didier, B. T.; Elsethagen, T.; Sun, L.; Gurumoorthi, V.; Chase, J.; Li, J.; Windus, T. L. Basis Set Exchange: A Community Database for Computational Sciences. *J. Chem. Inf. Model.* **2007**, *47*, 1045−1052.
(86) Boys, S. F.; Bernardi, F. Calculation of Small Molecular Interactions by Differences of Separate Total Energies - Some Procedures with Reduced Errors. *Mol. Phys.* **1970**, *19*, 553−566.
(87) Noro, T.; Sekiya, M.; Koga, T. Segmented contracted basis sets for atoms H through Xe: Sapporo-(DK)-nZP sets (n = D, T, Q). *Theor. Chem. Acc.* **2012**, *131*, 1124.
(88) Frisch, M. J.; Trucks, G. W.; Schlegel, H. B.; Scuseria, G. E.; Robb, M. A.; Cheeseman, J. R.; Scalmani, G.; Barone, V.; Petersson, G. A.; Nakatsuji, H.; et al. *Gaussian 16*, Rev. C.01: Wallingford, CT, 2016.
(89) Keith, A. T. *AIMAll* (Version 14.11.23), TK Gristmill Software: Overland Park KS, USA, 2014.
(90) te Velde, G.; Bickelhaupt, F. M.; Baerends, E. J.; Fonseca Guerra, C.; Van Gisbergen, S. J. A.; Snijders, J. G.; Ziegler, T. Chemistry with ADF. *J. Comput. Chem.* **2001**, *22*, 931−967.
(91) Stasyuk, O. A.; Sedlak, R.; Guerra, C. F.; Hobza, P. Comparison of the DFT-SAPT and Canonical EDA Schemes for the Energy Decomposition of Various Types of Noncovalent Interactions. *J. Chem. Theory Comput.* **2018**, *14*, 3440−3450.
(92) Lu, T.; Chen, F. Quantitative analysis of molecular surface based on improved Marching Tetrahedra algorithm. *J. Mol. Graph. Model.* **2012**, *38*, 314−323.
(93) Lu, T.; Chen, F. Multiwfn: a multifunctional wavefunction analyzer. *J. Comput. Chem.* **2012**, *33*, 580−592.
(94) Humphrey, W.; Dalke, A.; Schulten, K. VMD: Visual molecular dynamics. *J. Mol. Graph. Model.* **1996**, *14*, 33−38.
(95) Prima, D. O.; Vorontsova, E. V.; Makarov, A. G.; Makarov, A. Y.; Bagryanskaya, I. Y.; Mikhailovskaya, T. F.; Slizhov, Y. G.; Zibarev, A. V. Halogenated (F, Cl) 1,3-benzodiazoles, 1,2,3-benzotriazoles, 2,1,3-benzothia(selena)diazoles and 1,4-benzodiazines inducing Hep2 cell apoptosis. *Mendeleev Commun.* **2017**, *27*, 439−442.
(96) Macrae, C. F.; Bruno, I. J.; Chisholm, J. A.; Edgington, P. R.; McCabe, P.; Pidcock, E.; Rodriguez-Monge, L.; Taylor, R.; van de Streek, J.; Wood, P. A. Mercury CSD 2.0 - new features for the visualization and investigation of crystal structures. *J. Appl. Crystallogr.* **2008**, *41*, 466−470.
(97) Chivers, T. *A Guide to Chalcogen−Nitrogen Chemistry*; World Scientific: London (Singapore), 2005.
(98) Fourmigué, M.; Dhaka, A. Chalcogen bonding in crystalline diselenides and selenocyanates: From molecules of pharmaceutical interest to conducting materials. *Coord. Chem. Rev.* **2020**, *403*, 213084.
(99) Nakamoto, K. *Infrared and Raman Spectra of Inorganic and Coordination Compounds, Part B.*; Wiley & Sons Inc.: New York, 2009.
(100) Socrates, G. *Infrared and Raman Characteristic Group Frequencies: Tables and Charts*; John Wiley & Sons: Chichester, 2004.

https://dx.doi.org/10.1021/acs.jpca.0c10814
J. Phys. Chem. A 2021, 125, 657−668

(101) Siivari, J.; Chivers, T.; Laitinen, R. S. Synthesis and Characterization of Selenium Nitrogen Chlorides - Force-Field Calculations for the Se3n2cl+ Cation. *Inorg. Chem.* **1993**, *32*, 4391−4395.
(102) Alvarez, S. A cartography of the van der Waals territories. *Dalton Trans.* **2013**, *42*, 8617−8636.
(103) Zierkiewicz, W.; Wysokiński, R.; Michalczyk, M.; Scheiner, S. Chalcogen bonding of two ligands to hypervalent YF4 (Y = S, Se, Te, Po). *Phys. Chem. Chem. Phys.* **2019**, *21*, 20829−20839.
(104) Bader, R. *Atoms in Molecules. A Quantum Theory*; Clarendon Press: Oxford, 1990.
(105) Bader, R. F. W. A bond path: A universal indicator of bonded interactions. *J. Phys. Chem. A* **1998**, *102*, 7314−7323.
(106) Bader, R. F. W.; Essén, H. The Characterization of Atomic Interactions. *J. Chem. Phys.* **1984**, *80*, 1943−1960.
(107) Baryshnikov, G. V.; Minaev, B. F.; Minaeva, V. A.; Podgornaya, A. T.; Ågren, H. Application of Bader's atoms in molecules theory to the description of coordination bonds in the complex compounds of Ca2+ and Mg2+ with methylidene rhodanine and its anion. *Russ. J. Gen. Chem.* **2012**, *82*, 1254−1262.
(108) Contreras-Garcia, J.; Johnson, E. R.; Keinan, S.; Beratan, D. N.; Yang, W. T. From density to scoring functions: Revealing non covalent interactions. *Abstracts of Papers of the American Chemical Society*, 2011; Vol. *241*.
(109) Contreras-García, J.; Johnson, E. R.; Keinan, S.; Chaudret, R.; Piquemal, J.-P.; Beratan, D. N.; Yang, W. NCIPLOT: A Program for Plotting Noncovalent Interaction Regions. *J. Chem. Theory Comput.* **2011**, *7*, 625−632.
(110) Sánchez-Sanz, G.; Trujillo, C. Improvement of Anion Transport Systems by Modulation of Chalcogen Interactions: The influence of solvent. *J. Phys. Chem. A* **2018**, *122*, 1369−1377.
(111) Michalczyk, M.; Zierkiewicz, W.; Wysokiński, R.; Scheiner, S. Theoretical Studies of IR and NMR Spectral Changes Induced by Sigma-Hole Hydrogen, Halogen, Chalcogen, Pnicogen, and Tetrel Bonds in a Model Protein Environment. *Molecules* **2019**, *24*, 3329.
(112) Lu, J.; Scheiner, S. Effects of Halogen, Chalcogen, Pnicogen, and Tetrel Bonds on IR and NMR Spectra. *Molecules* **2019**, *24*, 2822.
(113) Scheiner, S.; Michalczyk, M.; Zierkiewicz, W. Structures of clusters surrounding ions stabilized by hydrogen, halogen, chalcogen, and pnicogen bonds. *Chem. Phys.* **2019**, *524*, 55−62.
(114) Scheiner, S.; Lu, J. Halogen, Chalcogen, and Pnicogen Bonding Involving Hypervalent Atoms. *Chemistry* **2018**, *24*, 8167−8177.
(115) Adhikari, U.; Scheiner, S. Effects of charge and substituent on the S···N chalcogen bond. *J. Phys. Chem. A* **2014**, *118*, 3183−3192.
(116) Azofra, L. M.; Scheiner, S. Substituent Effects in the Noncovalent Bonding of SO2 to Molecules Containing a Carbonyl Group. The Dominating Role of the Chalcogen Bond. *J. Phys. Chem. A* **2014**, *118*, 3835−3845.
(117) Esrafili, M. D.; Sadr-Mousavi, A. Chalcogen bonds tuned by an N-H center dot center dot center dot pi or C-H center dot center dot center dot pi interaction: investigation of substituent, cooperativity and solvent effects. *Mol. Phys.* **2017**, *115*, 1713−1723.
(118) Galmés, B.; Juan-Bals, A.; Frontera, A.; Resnati, G. Charge-Assisted Chalcogen Bonds: CSD and DFT Analyses and Biological Implication in Glucosidase Inhibitors. *Chem.—Eur. J.* **2020**, *26*, 4599−4606.
(119) Guo, X.; Liu, Y.-W.; Li, Q.-Z.; Li, W.-Z.; Cheng, J.-B. Competition and cooperativity between tetrel bond and chalcogen bond in complexes involving F2CX (X = Se and Te). *Chem. Phys. Lett.* **2015**, *620*, 7−12.
(120) Esrafili, M. D.; Mousavian, P.; Mohammadian-Sabet, F. The influence of hydrogen- and lithium-bonding on the cooperativity of chalcogen bonds: A comparative ab initio study. *Mol. Phys.* **2019**, *117*, 726−733.
(121) Esrafili, M. D.; Mousavian, P.; Mohammadian-Sabet, F. Tuning of pnicogen and chalcogen bonds by an aerogen-bonding interaction: a comparative ab initio study. *Mol. Phys.* **2019**, *117*, 58−66.
(122) Mó, O.; Montero-Campillo, M. M.; Alkorta, I.; Elguero, J.; Yez, M. Ternary Complexes Stabilized by Chalcogen and Alkaline-Earth Bonds: Crucial Role of Cooperativity and Secondary Non-covalent Interactions. *Chem.—Eur. J.* **2019**, *25*, 11688−11695.

https://dx.doi.org/10.1021/acs.jpca.0c10814
J. Phys. Chem. A 2021, 125, 657−668